Experimental and Numerical Study of Nonlinear Galloping oscillations Interfering with Vortex-Induced Excitation

Claudio Mannini*, Tommaso Massai* and Antonino Maria Marra*
*CRIACIV/Department of Civil and Environmental Engineering, University of Florence, Italy

Summary. This paper deals with the fascinating phenomenon of interference of two nonlinear fluid-elastic phenomena, viz. vortex-induced vibration (VIV) and transverse galloping. The resulting phenomenon, which one may call "unsteady galloping", occurs in the case of low-damped rectangular cylinders with a side ratio comprised between about 0.75 and 3. The results of a wide experimental campaign carried out in the wind tunnel on a rectangular 3:2 cylinder (having the short side perpendicular to the flow) are discussed here, with a special focus on the role played by the mass-damping parameter of the oscillating body. Moreover, the problem is analytically addressed through an existing nonlinear wake-oscillator model, which has been modified in the present work, especially concerning the setting of a key parameter, obtaining previously unexplored solutions of the equations. The model was found to reproduce correctly several features of the complicated phenomenon, shedding some light on the mechanism of unsteady galloping. Finally, the nonlinear behavior of the wake has also been discussed.

Introduction

Vortex-induced vibration (VIV) and transverse galloping are well-known nonlinear phenomena characterizing slender bluff bodies immersed in a flow stream. The former is a high-reduced frequency excitation triggered by vortex resonance, whilst the latter is generally a low-reduced frequency instability addressed with the well-established quasi-steady theory [1]. Nevertheless, as first noticed by Parkinson and Wawzonek [2], then by Bearman *et al.* [3], and recently extensively discussed in [4, 5], if the mass-damping parameter (often called Scruton number) is low enough, the ranges of excitation of the two phenomena tend to approach, and a peculiar type of instability occurs, with important implications from the engineering point of view [4, 6], since large-amplitude vibrations are observed in flow-speed ranges wherein no excitation is predicted by the classical theories of VIV and galloping. In particular, this has been observed for rectangular cylinders with a cross-sectional side ratio comprised between about 0.75 and 3 [7].
In the present work, a rectangular cylinder with a side ratio of 1.5 (having the short side perpendicular to the flow) has been the object of an extensive experimental and numerical investigation. For the sake of brevity, the results discussed here are those in smooth flow only, but the phenomenon of unsteady galloping also occurs in turbulent flow, showing specific features in that case [8].

Experimental study

The phenomenon of interference of Kármán vortex shedding and galloping was experimentally studied in the CRIACIV wind tunnel in Prato, Italy. A plywood sectional model of a rectangular cylinder was employed with a cross-section short side D of 77 mm, a long side B of 116 mm, and a spanwise length L of 986 mm. The model was provided with rectangular end-plates to enforce time-averaged two-dimensional flow conditions. Its carbon-fiber axis-tube was either clamped at the ends by a pair of six-component strain-gauges force balances (static tests) or elastically suspended through two shear-type frames of leaf springs (dynamic tests) to allow for the transverse degree of freedom only. Further details on the experimental setups can be found in [7].
Static tests were carried out to measure the drag and lift coefficients (respectively C_D and C_L), which allow determining the transverse force coefficient (see Figure 1), as follow:

$$C_{Fy}^{QS}(\alpha) = sec(\alpha)[C_L(\alpha) + C_D(\alpha)\, tan(\alpha)] \tag{1}$$

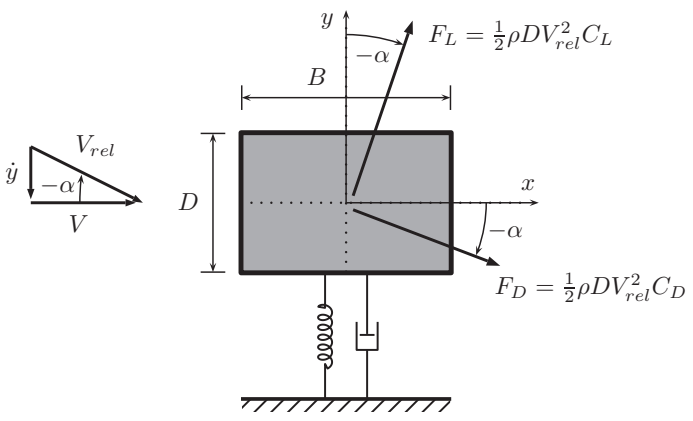

Figure 1: Schematic of the problem and determination of the transverse force on the vibrating rectangular cylinder with the quasi-steady approach.

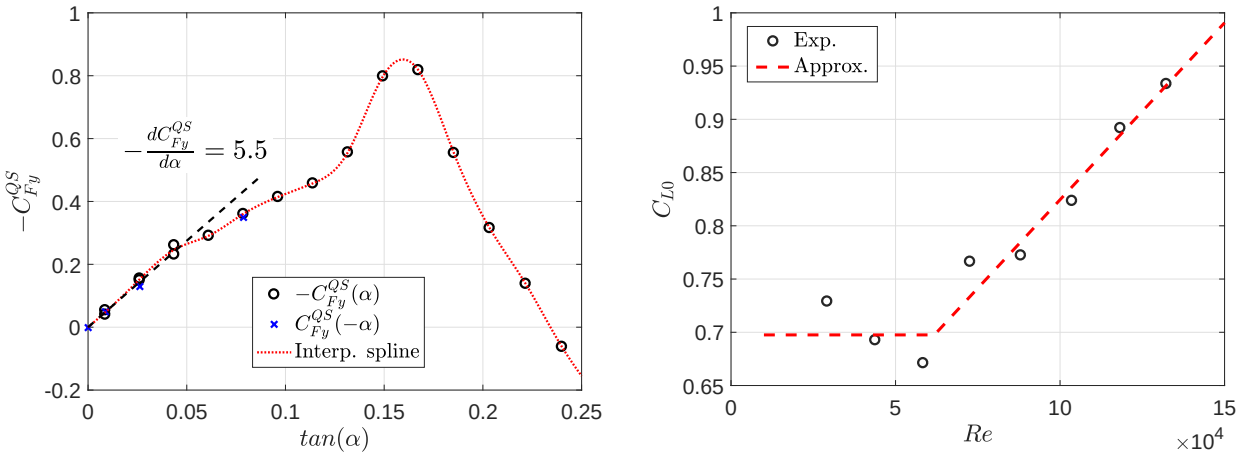

(a) (b)

Figure 2: (a) Experimental transverse force coefficient vs. angle of attack along with a cubic spline interpolation; (b) experimental coefficient C_{L0} vs. Reynolds number and a piecewise-linear approximation.

where α is the flow angle of attack, positive nose-up. C_{Fy}^{QS} is supposed to rule the quasi-steady galloping behavior [1]. No significant Reynolds number effects were detected. The Strouhal number St was also identified from force and wake measurements. It was found that this important parameter, which determines the onset of vortex-induced vibrations, takes a value of 0.106 for the present geometry. Finally, static tests enabled the identification of the fluctuation amplitude of the lift coefficient at the Strouhal frequency, C_{L0}. Such a parameter was obtained by integrating the power spectral density of the lift coefficient in a narrow band around the vortex-shedding frequency, and by multiplying the square root of the so-obtained variance times $\sqrt{2}$ (sinusoidal equivalent amplitude). Figure 2(b) highlights that significant Reynolds number effects were observed.

In the dynamic tests, the damping of the system was varied in small steps through eddy-current dampers, so to explore a wide range of values of the mass damping parameter. The latter, called Scruton number Sc, is here defined as 4π times the mechanical critical damping ratio ζ_0 times the mass of the oscillating system M, normalized with the mass of air occupying the volume of the rectangular prism:

$$Sc = \frac{4\pi M \zeta_0}{\rho B D L} \tag{2}$$

The linearity of the system in still-air was verified beforehand up to high amplitudes of oscillation.

Results for several values of the Scruton number are shown in Figure 3. In spite of a ratio of the quasi-steady galloping critical flow speed U_g to the vortex-resonance flow speed U_r larger than 1.6, for $Sc = 28$ a fully combined excitation occurs, the instability arising at the vortex-resonance flow speed, and then the oscillation amplitude monotonically growing in a nearly linear fashion. For Scruton numbers equal to 37 and 41 (respectively $U_g/U_r = 2.15$ and 2.42), a transitional behavior is observed: the first part of the amplitude-velocity curve is exactly the same as for lower Scruton numbers, but then a peak amplitude and a plateau region are encountered, before the response curve suddenly jumps up to a higher instability branch with a large hysteresis loop. It is to note that the quasi-steady instability threshold seems to coincide with the lower bound of the hysteresis loop. For Scruton numbers equal to 46 and 52 (respectively $U_g/U_r = 2.68$ and 3.02), no hysteresis loops are visible and, after the local maximum in the amplitude-velocity curve in the vortex-resonance region, a range of small (but still significant) and irregular vibrations is observed. At higher velocities, though lower than the quasi-steady threshold, large-amplitude oscillations appear again. High values of the mass-damping parameter ($Sc \sim 60$, $U_g/U_r \sim 3.5$) have to be reached for a full separation of the excitation mechanisms of vortex-induced vibration and galloping.

On the other hand, for low values of the Scruton number, when $U_g/U_r < 1$, vortex shedding is able to prevent the onset of galloping instability, according to the phenomenon known as "asynchronous quenching" [9]. For high Scruton numbers (46 and 52 in Figure 3), a super-harmonic resonance of order 3 is also apparent, in line with the findings in [3] for a square cylinder. Finally, it is worth remarking the self-limited excitation occurring at low-reduced flow velocity for low values of the Scruton number. It has been conjectured and discussed in [7] that these are vortex-induced vibrations due to a secondary mechanism of vortex shedding.

Numerical analysis

The combined effect of Kármán-vortex shedding and galloping instability was also numerically investigated by applying the wake-oscillator model proposed by Tamura and Matsui [10] for a circular cylinder and then adapted to a square cylinder by Tamura and Shimada [11]. The model is based on Birkhoff's idea of the wake as a swinging lamina [12], and it relies on a simple linear superposition of quasi-steady and unsteady-wake nonlinear forces. In the present work,

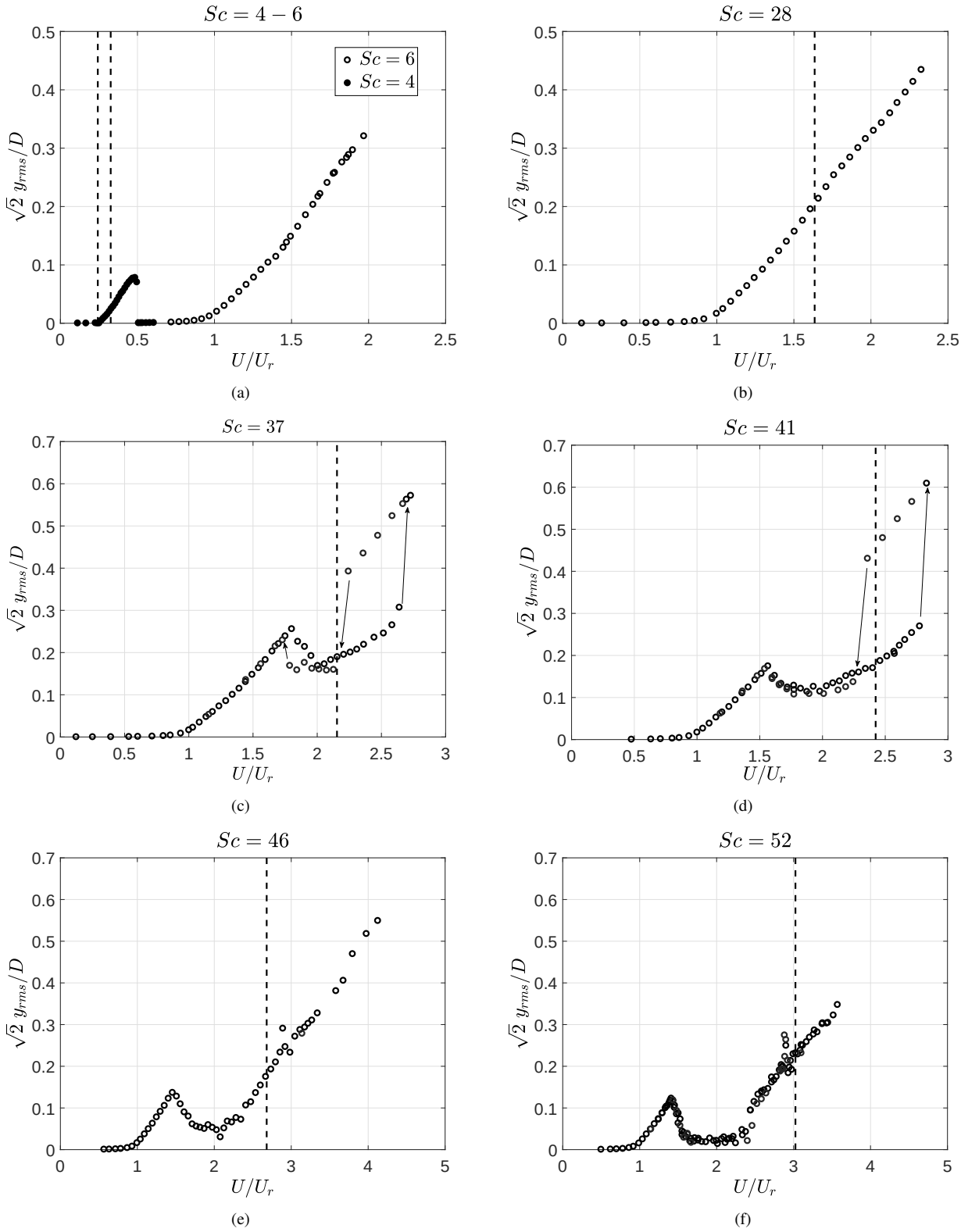

Figure 3: Steady-state amplitude-velocity curves for several values of the mass-damping parameter. The dashed lines indicate the quasi-steady instability thresholds.

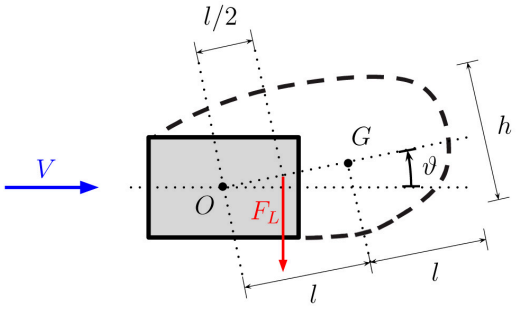

Figure 4: Schematics of modified Tamura and Shimada's model.

the governing equations were slightly modified for theoretical reasons. In particular, considering that for a rectangular cylinder with a side ratio close to unity the wake is not expected to pivot about the stagnation point, but it starts swinging slightly downstream, we decided to go back to Birkhoff's formulation (the wake lamina is assumed to pivot around the center of the cylinder), at variance with Tamura and Shimada's scheme [11]. In addition, coherently with the equivalent wake lamina assumption, we considered the lift force acting on it to be applied at one fourth of its length, thus removing an unexplained modification introduced by Funakawa [13]. Therefore, the wake oscillator considered herein is that schematized in Figure 4, and expressed by the equations:

$$Y'' + 2\zeta_0 Y' + Y = -m^* \frac{U^2}{4\pi^2} f \left(\vartheta + \frac{2\pi Y'}{U} \right) - m^* \frac{U^2}{4\pi^2} C_{Fy}^{QS} \tag{3}$$

$$\vartheta'' - 2\beta \upsilon \vartheta' \left(1 - \frac{4f^2}{C_{L0}^2} \vartheta^2 \right) + \upsilon^2 \vartheta = -\lambda Y'' - \upsilon^2 \frac{2\pi Y'}{U} \tag{4}$$

where $U = V/n_0 D$ is the reduced flow speed, V the incoming flow speed, n_0 the still-air natural transverse vibration frequency, ζ_0 the critical mechanical damping ratio, $m^* = \rho D^2 L/2M$ the mass ratio, M the mass of the body. $\upsilon = USt = U/U_r = n_s/n_0$ is the velocity ratio with respect to the Kármán-vortex-resonance flow speed $U_r = 1/St$ (or frequency ratio), and C_{L0} the amplitude of the lift coefficient fluctuation for the stationary cylinder. The quasi-steady transverse force coefficient C_{Fy}^{QS} is a function of the apparent flow angle of attack α, where $tan(\alpha) = -2\pi Y'/U$. In addition, it holds:

$$\beta = \frac{4\sqrt{2}}{\pi} St^2 h^* f \tag{5}$$

$$\lambda = 8\pi St^2 h^* \tag{6}$$

being f the slope of the unsteady vortex-excited lift coefficient with respect to the wake inclination ϑ. In addition, the normalized length $2l^* = 2l/D$ of the equivalent wake lamina (see Figure 4) has to satisfy the following equation:

$$l^* h^* = \frac{1}{8\pi St^2} \tag{7}$$

Clearly, Eq. (4) denotes a Van-der-Pol-type oscillator coupled to the body oscillator (Eq. (3)) through the forcing terms. In addition, the model was derived from physical principles and assumptions instead of being based on empirical and mathematical considerations as for other approaches (e.g. [14]).

It is worth noting that, from the analytical point of view, the present version of the model slightly differs from the original one [11] only for the expressions of the derived parameters β and λ, as well as for Eq. (7).

Another crucial modification of the original model introduced in the present work is the definition of the parameter f. Tamura and Shimada [11] related f to the Magnus effect for a rotating cylinder, although for a sharp-edged body the analogy is questionable and surely not straightforward. They used the value $f = 1.16$, derived for a circular cylinder by Funakawa [13], and only outlined a sensitivity study on it. This approach was abandoned here. Instead, f was calibrated based on the experimental dynamical response in the pure VIV regime, for a high value of the mass-damping parameter, that is with no complicated interference with the galloping instability. It will be clear later that this choice has very important consequences on the behavior of the equations.

The model equations (Eqs. (3)-(4)) were numerically solved by means of ODE45 Matlab® function, employing the explicit Runge-Kutta method and specifically the Dormand-Prince algorithm, which uses six function evaluations to calculate fourth- and fifth-order accurate solutions. Some control parameters, such as relative and absolute tolerances, were properly tuned beforehand, so to optimize the accuracy of the solution. Several different initial conditions were considered to explore the possible presence of multiple stable solutions in the range of amplitudes of interest for the reference wind tunnel tests [7] and for most practical applications.

h^*, f, St, C_{L0} and $C_{Fy}^{QS}(\alpha)$ in Eqs. (3)-(6) are the model's aerodynamic parameters that have to be set in the equations. The appealing feature of the model is that all these parameters have a precise physical meaning. In particular, all parameters but h^* and f can be easily determined through simple experimental static tests on a cylinder held stationary.

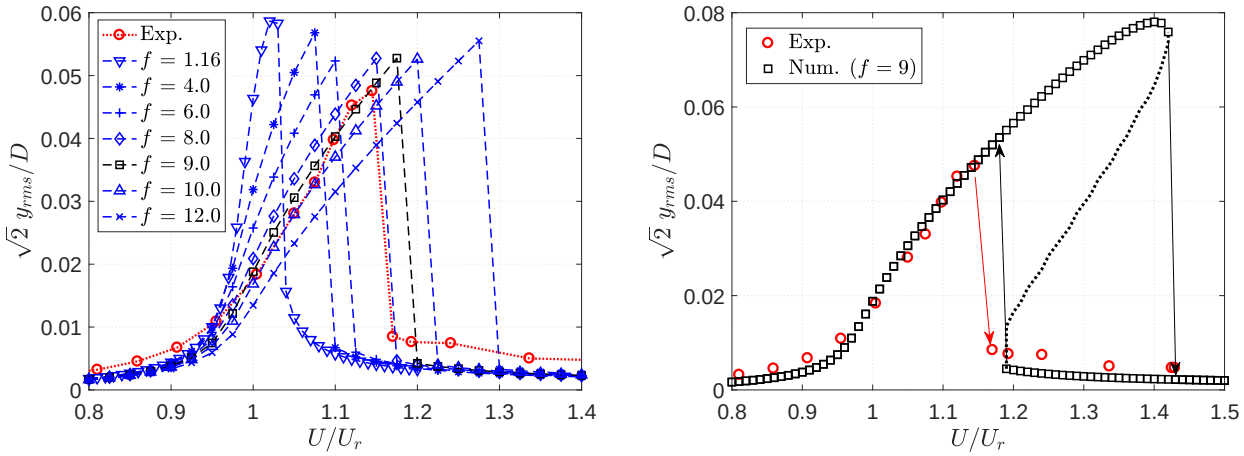

(a) (b)

Figure 5: (a) Numerical results for $Sc = 86$ obtained setting different values of the parameter f and considering a small perturbation of the zero-amplitude solution as initial condition; (b) numerical results obtained setting $f = 9$ for various initial conditions (the dotted line denotes the unstable solution branch).

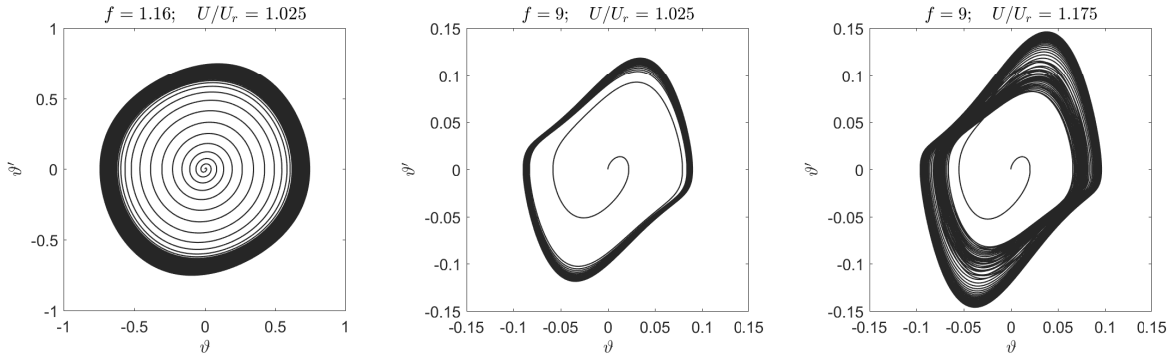

(a) (b) (c)

Figure 6: Phase-space diagrams of the evolution of the variable ϑ from the initial condition $Y(0) = 0.01$, $Y'(0) = 0$, $\vartheta(0) = 0$, $\vartheta'(0) = 0$: at the reduced flow speed corresponding to the peak-amplitude in the VIV range for $f = 1.16$ (a); at the same reduced flow speed as in (a) but for $f = 9$ (b); at the reduced flow speed corresponding to the peak-amplitude in the VIV range for $f = 9$ (c).

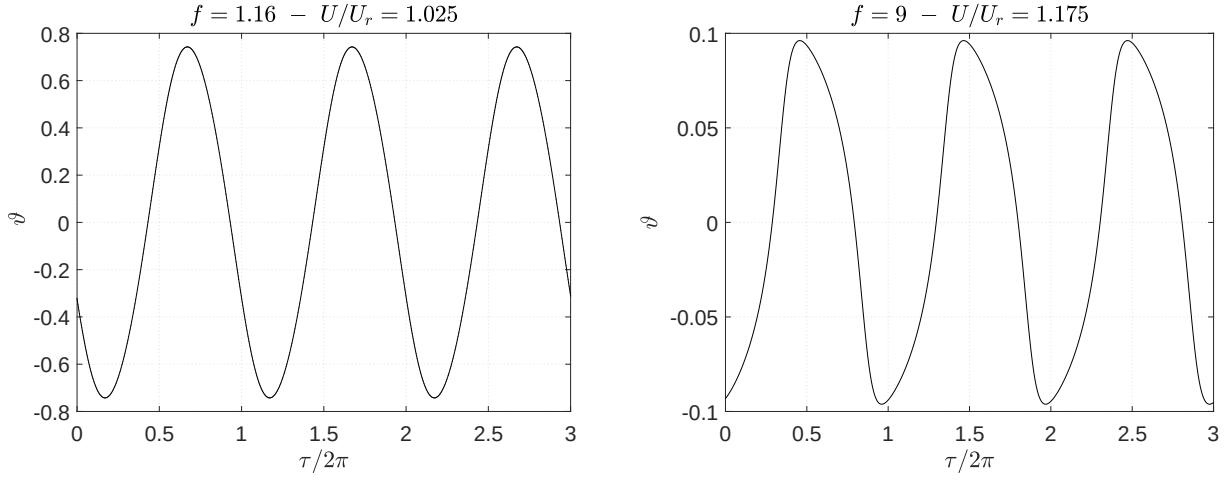

(a) (b)

Figure 7: Time histories of the steady-state wake oscillation at the reduced flow speed corresponding to the peak-amplitude in the VIV range for either $f = 1.16$ (a) or $f = 9$ (b).

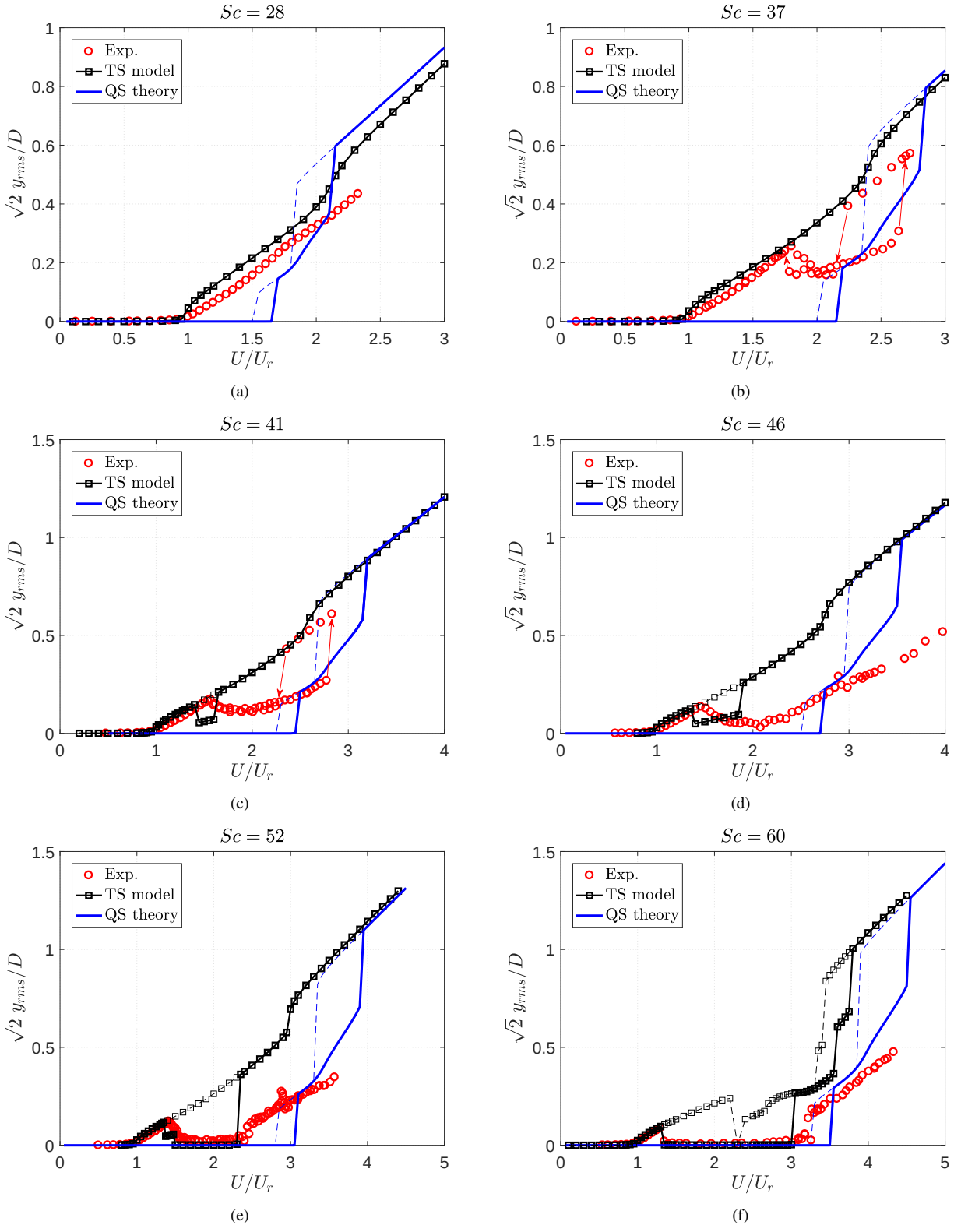

Figure 8: Comparison between experimental and numerical results (the latter denoted as "TS model") for various Scruton numbers. Heavy and light markers denote respectively lower- and upper-branch solutions of the equations. QS stands for "quasi-steady".

The experimental estimation of the nondimensional depth of the equivalent wake lamina $h^* = h/D$ (Figure 4) is more difficult. In fact, flow visualizations or time-accurate flow field measurements would be necessary but they are not available. Therefore, supported also by the numerical results reported in [15], it was decided to set $h^* = 1.8$, as in [11] for the square cylinder, and then to investigate the sensitivity of equations' results to variations of this parameter.
As for the calibration of the parameter f, a test case with a Scruton number of 86 was considered. f was varied in the range 0.5 to 12, and a selection of the resulting solutions of the equations is reported in Figure 5(a). A small perturbation of the zero-amplitude solution was assumed as initial condition. It can be noted that the peak amplitude of the VIV response is not much influenced by the value of f, whilst it is the slope of the amplitude-velocity curve and consequently the extension of the flow-speed range of excitation. In particular, this slope decreases for an increment of f. A value of f of about 9 leads to a good agreement with the experimental data, and therefore this is the value that was set in the equations in the following analysis. In contrast, Figure 5(b) shows the results obtained starting from various larger initial conditions. A large hysteresis loop at the upper bound of the VIV range is apparent in the numerical results, while it was not observed in the experiments [7]. It was also verified that the results obtained with the mathematical model are not sensitive to significant deviations from the nominal value of the parameter h^*, which is reassuring, given the uncertainty in its setting.
In the original version of the model, the value $f = 1.16$ was set in the equations, relying on the previously mentioned analogy with the Magnus effect for a rotating cylinder. This implies a value of β nearly one order of magnitude smaller than what obtained here (see Eq (5)). This also means that the Van-der-Pol-type equation for the wake oscillator behaves as a weakly nonlinear equation in the original version of the model, while it shows pronounced nonlinear features in the present formulation ($2\beta = 0.08$ and 0.65 respectively for $f = 1.16$ and 9). This difference is clear in the results reported in Figures 6-7. As a consequence, with the low value of f set in the equations by Tamura and Shimada [11], the synchronization range results to be excessively narrow (Figure 5(a)), and the tendency of vortex shedding and galloping to interfere is expected to be limited. In addition, a low value of f implies very large-amplitude of oscillation of the wake lamina (up to nearly 1 rad), in contradiction with the physical assumptions on which the model is based (see [10]). Conversely, the oscillations of ϑ are much smaller for $f = 9$ (around 0.1 rad).
Results for several values of the mass-damping parameter are reported in Figure 8, where a comparison with the experimental data is also provided. The model is able to predict the dynamical response of the rectangular cylinder with satisfactory agreement with the experimental data. In particular, it captures the onset of the oscillations around the vortex-resonance flow speed and the nearly linear increase of the steady-state amplitude of the motion (Figure 8(a)), without the large overshoot around the vortex resonance observed in [11], or in [14] with a similar mathematical model. In contrast, some limitations were observed in the Scruton number range for which transition in the interference phenomenon occurs, the numerical results overestimating the value of the mass-damping parameter up to which the amplitude-velocity curve monotonically increases (Figure 8(b)). The hysteresis loops observed in the experiments in the developed galloping velocity range are instead shown by the model immediately after the VIV region, even for high values of the Scruton number (namely $Sc = 46$, 52 and 60, Figures 8(d)-8(f)), for which no evidence of a hysteretic behavior was found in the wind tunnel tests. Moreover, though not shown in the figures, one may note that the mathematical model's results present a slope of the amplitude-velocity curves that tends to increase for very low values of the Scruton number, in contrast with the experimental results in [4, 7]. Nevertheless, such a behavior was observed in [6] for a three-dimensional arch structure with the same 3:2 cross section.
The behavior of the wake oscillator is further investigated for $Sc = 46$ in Figure 9(a), where the dominant frequency in the time histories of ϑ is plotted against the velocity ratio U/U_r. It is to note that the Strouhal law is followed up to the

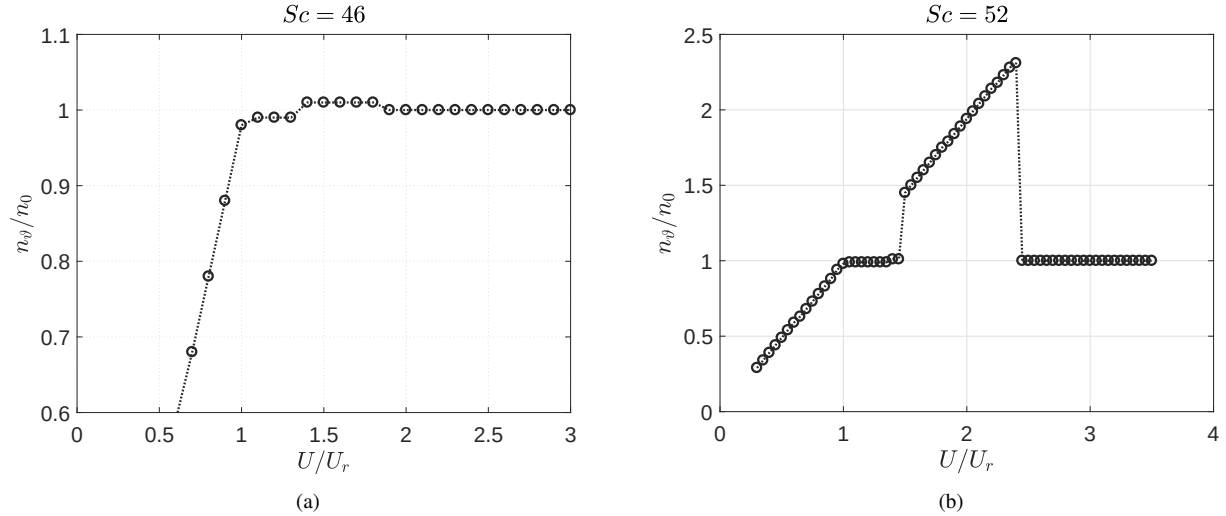

(a) (b)

Figure 9: Pattern of the dominant wake frequency vs. reduced flow speed for two values of the Scruton number (the lower branch is considered in the hysteresis loops).

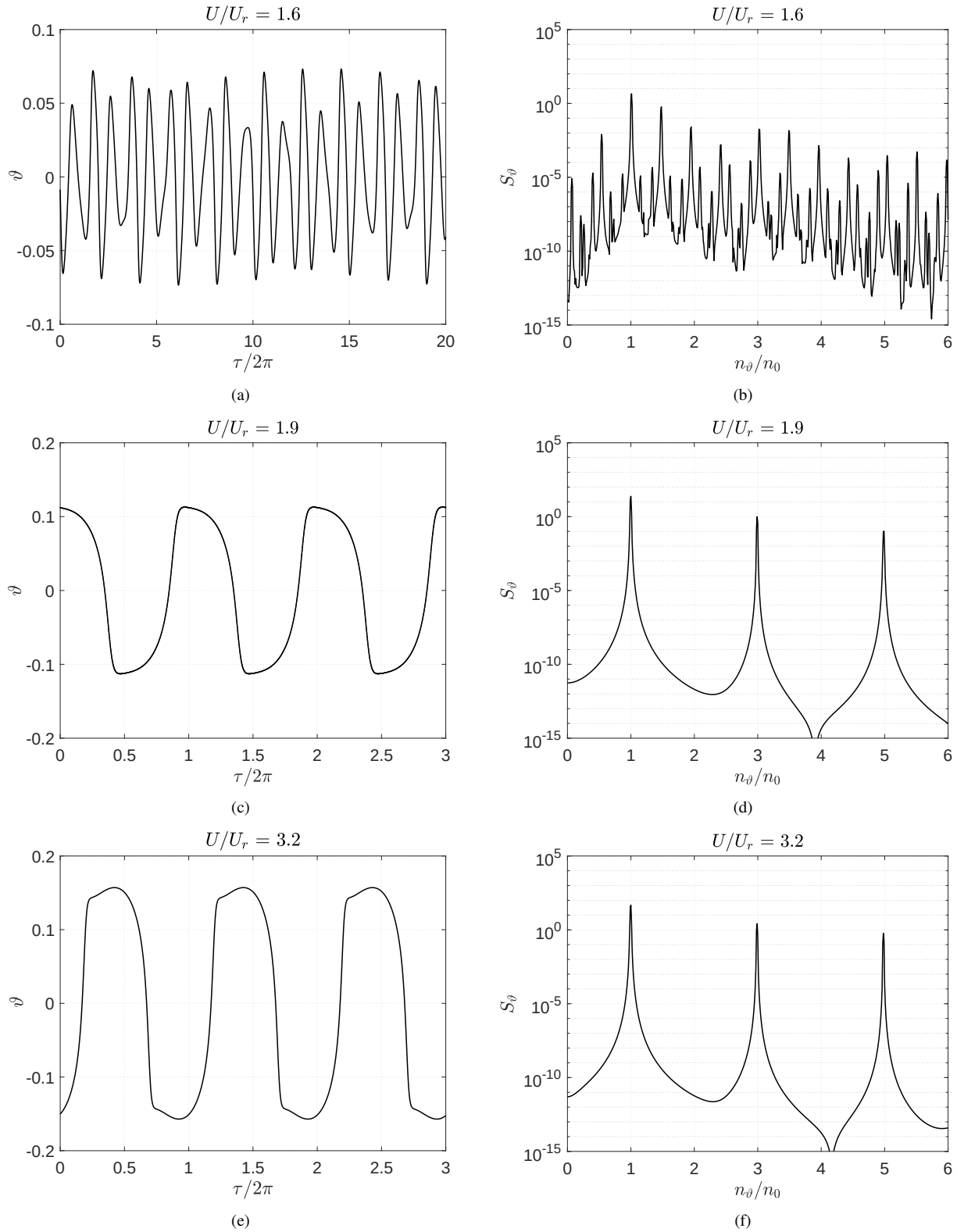

Figure 10: Time histories (left frames) and corresponding power spectral densities (right frames) of the steady-state wake oscillation at two reduced flow speeds for $Sc = 46$ (the lower branch is considered in the hysteresis loops).

vortex-resonance flow speed ($U/U_r = 1$), when the wake frequency synchronizes with the body oscillator at a frequency slightly lower than n_0. Then, in the lower branch of the hysteresis loop observed for $1.4 \lesssim U/U_r \lesssim 1.9$, the frequency becomes slightly larger than the still-air body-oscillator one, and finally it takes exactly the value n_0 in the developed galloping branch, for $U/U_r \gtrsim 1.4$. For a slightly larger Scruton number ($Sc = 52$), Figure 9(b) clarifies that the model predicts that the Strouhal law is recovered in the wake when the oscillations go down to zero after the lock-in region, although with a slightly lower frequency than for $U/U_r < 1$.

Some evidences of the strong nonlinear behavior of the wake oscillator are shown in Figure 10, where the significant contribution of odd superharmonics is apparent in the time histories (Figures 10(e) and 10(f)). One can also appreciate the

complicated, non-perfectly periodic, behavior observed in the lower branch of the hysteresis loop for $Sc = 46$ (namely for $U/U_r = 1.6$), in a similar way to what emphasized by the experiments [7]. In addition, it is interesting to remark that the oscillations of ϑ are relatively small even for large-amplitude vibration of the body oscillator (Figure 10(e)).

Conclusions and prospects

Wind tunnel tests revealed that the rectangular cylinder with a side ratio of 1.5 is very prone to the interference of VIV and transverse galloping. High values of the mass-damping parameter are required to decouple the two excitation mechanisms, and complicated nonlinear features occur in the transitional range of Scruton numbers.
The unsteady-galloping phenomenon was also approached through a modified version of the wake-oscillator model proposed by Tamura and co-workers, which is able to reproduce the main features of these flow-induced vibrations. In particular, the completely different setting of a parameter in the model allowed for a more pronounced nonlinear behavior of the wake oscillator, enabling a stronger tendency to synchronization of the two coupled oscillators and a better agreement with the experimental results. In addition, the basic underlying assumption of the model, namely the linear superposition of quasi-steady and unsteady wake forces, provides a simple physical interpretation of the main excitation mechanism of the interference phenomenon. Nevertheless, the limitations of the model were also highlighted in the paper. A future development of the work might be the inclusion in the mathematical model of the effects of large-scale turbulence, affecting the system as both an external forcing and a parametric excitation.

References

[1] Parkinson G. V., Smith J. D. (1964) The square prism as an aeroelastic non-linear oscillator. *Q. J. Mech. Appl. Math.* **17**(2):225-239.

[2] Parkinson G. V., Wawzonek M. A. (1981) Some considerations of combined effects of galloping and vortex resonance. *J. Wind Eng. Ind. Aerodyn.* **8**(1-2):135-143.

[3] Bearman P. W., Gartshore I. S., Maull D. J., Parkinson G. V. (1987) Experiments on fluid-induced vibration of a square-section cylinder. *J. Fluids Struct.* **1**(1):19-34.

[4] Mannini C., Marra A. M., Bartoli G. (2014) VIV-galloping instability of rectangular cylinders: Review and new experiments. *J. Wind Eng. Ind. Aerodyn.* **132**:109-124.

[5] Mannini C., Marra A. M., Bartoli G. (2015) Experimental investigation on VIV-galloping interaction of a rectangular 3:2 cylinder. *Meccanica* **50**(3):841-853.

[6] Mannini C., Belloli, M., Marra A. M., Bayati I., Giappino S., Robustelli, F. Bartoli G. (2016) Aeroelastic stability of two long-span arch structures: A collaborative experience in two wind tunnel facilities. *Eng. Struct.* **119**:252-263.

[7] Mannini C., Marra A. M., Massai T., Bartoli G. (2016) Interference of vortex-induced vibration and transverse galloping for a rectangular cylinder. *J. Fluids Struct.* **66**:403-423.

[8] Mannini C., Marra A. M., Massai T., Bartoli G. (2017) Interference of vortex-induced vibration and galloping of a rectangular cylinder in turbulent flow. *Proc. 7th European and African Conference on Wind Engineering*, Liège, Belgium, 4-7 Jul. 2017.

[9] Minorsky N. (1947) Introduction to Non-Linear Mechanics: Topological Methods, Analytical Methods, Non-Linear Resonance, Relaxation Oscillations. J. W. Edwards, Ann Arbor, US.

[10] Tamura Y., Matsui G. (1979) Wake-oscillator model of vortex-induced oscillation of circular cylinder. *Proc. 5th International Conference on Wind Engineering*, Forth Collins, US, 8-14 Jul. 1979:1085-1094.

[11] Tamura Y., Shimada K. (1987) A mathematical model for the transverse oscillations of square cylinders. *Proc. 1st International Conference on Flow Induced Vibrations*, Bowness-on-Windermere, UK, 12-14 May 1987:267-276.

[12] Birkhoff G. (1953) Formation of vortex streets. *J. Appl. Phys.* **24**(1):98-103.

[13] Funakawa M. (1969) The vibration of a cylinder caused by wake force in a flow. *B. Jpn. Soc. Mech. Eng.* **12**(53):1003-1010.

[14] Corless R. M., Parkinson G. V. (1988) A model of the combined effects of vortex-induced oscillation and galloping. *J. Fluids Struct.* **2**(3):203-220.

[15] Shimada K., Ishihara T. (2002) Application of a modified $k-\epsilon$ model to the prediction of aerodynamic characteristics of rectangular cross-section cylinders. *J. Fluids Struct.* **16**(4):465-485.